3D-Printed High Data-Density Electromagnetic Encoders Based on Permittivity Contrast for Motion Control and Chipless-RFID

Cristian Herrojo, *Member IEEE*, Ferran Paredes, *Member IEEE*, Jordi Bonache, *Member* IEEE, and Ferran Martín, *Fellow IEEE*

Abstract— **3D-printed electromagnetic encoders based on permittivity contrast are presented and discussed in this paper. The encoders, implemented by using exclusively dielectric materials, are based on linear chains of dielectric inclusions. Two types of encoders are considered: (i) those where the inclusions are simple apertures made on a 3D-printed dielectric plate (or substrate), and (ii) those with inclusions made of high dielectric constant material 3D-printed on a dielectric substrate (also 3D-printed). In both cases, encoding is achieved by varying the dielectric constant of the substrate at predefined positions by means of the inclusions. For encoder reading, a microstrip line loaded with a slot resonator (etched in the ground plane) and a series gap is proposed. Such structure is very sensitive to short range dielectric constant variations, being able to detect the presence or absence of closely spaced inclusions when the encoder is displaced on top of the sensitive part of the reader, the slot resonator. For that purpose, the reader line is fed by a harmonic signal conveniently tuned, so that an amplitude modulated (AM) signal containing the ID code is generated at the output port of the line. The proposed reader/encoder system is useful for motion control applications (linear displacement and velocity sensors) and for near-field chipless-RFID. Lower cost and major robustness against mechanical wearing are potential advantages of these encoders over other electromagnetic encoders based on a similar principle but based on metallic inclusions.**

Index Terms– **Microwave encoder, 3D-printing, additive manufacturing, chipless-RFID, motion control, microstrip technology, slot resonators.**

I. INTRODUCTION

Recently, electromagnetic encoders have been proposed as a low-cost alternative to optical encoders. In optical encoders, a grid of apertures in a metallic plate is used for coding purposes. The presence or absence of apertures during encoder motion is detected by means of an optical beam, and information relative to the displacement and velocity (either linear or angular) of the encoder can be inferred on the basis of pulse counting [1]-[3]. Optical encoders with very high resolution are available in the market and are of high interest in many industrial applications related to motion control (e.g., elevators, servomechanisms, automotive industry, etc.).

Despite the fact that it is difficult to compete against optical encoders in terms of spatial resolution (dictated by the grid period), such encoders have two main drawbacks: their cost (as well as the cost of the optical source and detector), and their limited robustness when they are subjected to certain harsh environments, e.g., with pollution, dirtiness, or grease, among others. The cost of the source/detection system can be reduced by using radiofrequencies (RF) or microwaves, rather than optical signals. However, the use of the RF/microwave spectrum needs a different strategy for encoder implementation. In [4]-[17], the proposed electromagnetic encoders were fabricated by etching or printing a chain of metallic inclusions (typically resonators or strips) on a dielectric substrate. In applications where mechanical robustness is required and the cost of the encoder is not critical, e.g., motion control, rigid substrates are preferable [4]-[7]. However, low-cost flexible substrates (including plastic or paper) can be used in applications where the cost of the encoder is a critical issue [10]-[13]. This applies to chipless-RFID, where ultra-low cost encoders (or tags) can be fabricated by printing the metallic inclusions through inkjet printing, or by means of massive fabrication processes (such as rotogravure, screen-printing, offset, etc.). Although the cost of commercially available conductive inks is moderately high, a very small quantity of ink suffices for tag fabrication. Thus, the price of printed encoders implemented on plastic or paper substrates is situated below the cost of chip-based tags, and, obviously, much below the cost of optical encoders.

As compared to optical encoders, electromagnetic encoders may offer major levels of confidence in certain industrial scenarios where the presence of contaminants or pollution may jeopardize the necessary cleanness and transparency of optical apertures. In chipless-RFID applications, the absence of chip in the tags (replaced by the metallic encoder), not only reduces costs, but it may also represent a good solution in scenarios subjected to extreme temperatures or radiation (e.g., integrated circuits exhibit limited radiation hardness). However, encoders based on printed metallic patterns may be subjected to wearing and aging effects that may limit their long-life use. Note that wearing may be caused by unexpected contacts (due, e.g., to vibration) between the encoder and the sensitive part of the reader (a RF/microwave component able to detect the presence of metallic inclusions through near-field).

In [18], we proposed a new type of low-cost electromagnetic encoders, based exclusively on dielectric materials, and thereby robust against wearing and aging

effects. In such encoders, the metallic chains of printed (or etched) resonant elements or strips are replaced with apertures in the substrate. Since the electromagnetic properties of the apertures (in particular the dielectric constant) are different from those of the substrate, such apertures are useful for coding purposes, as demonstrated in [18].

In the work presented in [18], the functionality of all-dielectric electromagnetic encoders based on permittivity contrast was demonstrated. However, the period of the apertures chain, similar to the size of the sensitive element of the reader, a complementary spiral resonator (CSR), was not optimized. Reduction of such period is fundamental since it dictates the sensor resolution (in the measurement of displacements and velocities) and the per unit length data density (a key parameter in encoders based on chains of inclusions for its use as chipless-RFID tags). In this paper, by designing (and optimizing) a completely new reader (i.e., the sensitive part), based on a linearly-shaped slot resonator, it is demonstrated that the period of the encoders can be substantially reduced. Moreover, we report not only all-dielectric encoders based on apertures (with linear shape), but also permittivity contrast encoders consisting of chains of high dielectric constant inclusions on top of a flexible dielectric substrate. In both cases, the encoders are fully fabricated through additive manufacturing by means of a 3D printer. All these aspects represent a significant extension and added contribution with regard to the idea and results first presented in [18]. Indeed, all the simulated and experimental results presented in this paper, as well as the reader and the different 3D-printed encoders, are original. Moreover, to the best of our knowledge, it is the first time that 3D-printed electromagnetic encoders are reported.

The proposed 3D-printed all-dielectric encoders are of interest for motion control applications, and for near-field chipless-RFID. In the former application, thick additive manufactured encoders based on periodically located apertures are suitable for measuring the relative position and velocity between the encoder and the reader. In this application, system robustness (related to the rigidity and hence thickness of the encoder) is a critical aspect. By contrast, in near-field chipless-RFID, encoder cost must be as much reduced as possible. For this reason, encoder implementation by 3D printing dielectric inclusions on a narrow and flexible substrate (also 3D-printed) is the preferred option for this second application.

The paper is organized as follows. The principle of operation of the proposed all-dielectric permittivity contrast encoders is presented in Section II. Section III focuses on the design of the sensitive part of the reader, a microstrip line loaded with slot resonator and series gap. The design is supported by a lumped element circuit model and by full-wave electromagnetic simulations. Section IV deals with the design of the encoders. System validation is reported in Section V, where the functionality of the encoders as displacement/velocity sensors, as well as chipless-RFID tags is demonstrated. This section also includes the description of the 3D-printing process and the considered materials. In section VI, a discussion related to the advantages and limitations of the proposed 3D-printed encoders, as compared to other encoders, is reported. Finally, the main conclusions are highlighted in Section VII.

II. WORKING PRINCIPLE

In the printed electromagnetic encoders based on metallic patterns reported in [4]-[17], a sensitive element able to detect the presence/absence of functional metallic elements (the inclusions) in the encoder chain was used for reading purposes. Specifically, encoder reading was carried out through near-field, by using a transmission line based structure, where such transmission line is typically loaded with a resonator (or resonators) sensitive to the presence of metallic elements in their surroundings.

Similarly, in all-dielectric encoders based on permittivity contrast, an element able to detect, through near-field, the presence/absence of dielectric inclusions (on the basis of dielectric constant variation), is needed [18]. For that purpose, a high-sensitive permittivity sensor, able to detect local changes in the permittivity of the encoder is a due. In [18], the permittivity contrast encoder was implemented by means of square apertures on a microwave (rigid) substrate, and the sensing element of the reader was a microstrip line loaded with a CSR, etched in the ground plane.

In this paper, a different sensing transmission line based structure, compatible with the detection of smaller (in the direction of the chain axis) dielectric inclusions, is proposed. Nevertheless, the principle is the same; namely, the presence of the inclusions on top of the sensitive element (a resonator) modifies the frequency response of the structure. Therefore, through encoder motion, an AM signal at the output port is generated, provided the line is fed with a conveniently tuned harmonic signal. The envelope of such AM signal, which can be obtained by means of an envelope detector, contains the relevant information, either relative to the displacement/velocity or to the identification (ID) code. For the measurement of the displacement and velocity, all the inclusions are present at the predefined positions in the encoder chain. Thus, the quasi-instantaneous velocity is determined from the time distance between adjacent peaks, or dips, in the envelope function, whereas the displacement is inferred from the cumulative number of peaks, or dips. In the functionality of the encoder as a chipless-RFID tag, only those dielectric inclusions associated to the logic level '1' are present. Thus the ID code is sequentially obtained by reading the envelope function at predefined time windows, where the amplitude of the envelope function determines the logic state, or bit, of the corresponding encoder position.

The sketch of the system is depicted in Fig. 1. It is worth mentioning that the frequency of the interrogation signal, f_c, must be tuned to a value providing a large excursion in the transmission coefficient, since this enhances the modulation index, hence representing major robustness against misalignments between the encoder and the reader or mechanical vibrations. An important difference of the proposed system, as compared to frequency domain [19]-[39], hybrid [40]-[51] and time-domain reflectometry (TDR) [52]-[65] chipless-RFID systems, is the fact that a
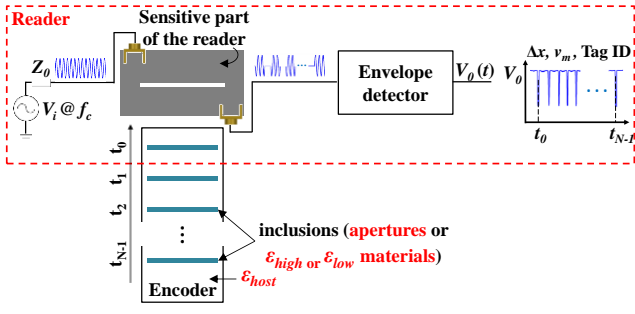
Fig. 1. Sketch of the proposed reader-encoder system. The inclusions of the encoder may be apertures, or high (or low) dielectric constant materials as compared with the dielectric constant of the host substrate, ε_{host}.
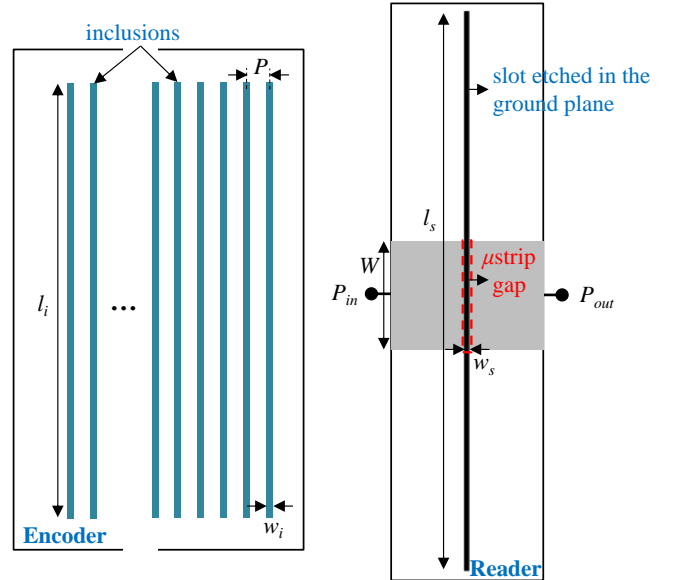

Fig. 2. Topology of the proposed reader-encoder and relevant dimensions (in mm). $W = 3.98$, $l_s = 24$, $w_s = 0.2$, $l_i = 18$, $w_i = 0.4$, and $P = 3.4$. In the encoder, the considered inclusions are linearly shaped apertures, but 3D-printed high (or low) dielectric constant material inclusions can be also considered.

single harmonic signal suffices for tag reading. By contrast, frequency sweeping and a pulsed signal is required for tag reading in frequency domain (and hybrid) and TDR based chipless-RFID systems, respectively. This represents further costs associated to the necessary electronics for the generation of the interrogation signal and for signal processing. Thus, in the proposed system, based on the amplitude modulation of the interrogation signal by encoder motion, low cost readers are envisaged, representing a clear advantage over traditional frequency-domain and TDR-based chipless-RFID systems.

As compared to previous electromagnetic encoders based on chains of metallic elements [4]-[17], the advantage of the proposed all-dielectric permittivity contrast encoders lies in the encoder side (rather than in the cost of the reader). Since conductive inks are not used, permittivity contrast encoders are more robust against wearing and aging effects. Moreover, implementing the encoders by means of apertures or dielectric inclusions is in general cheaper, as compared to metallic inclusions (either etched or printed through conductive inks).

III. READER DESIGN AND ANALYSIS

In the use of the encoder as displacement and velocity sensor, it is convenient to reduce the chain period as much as possible, since such period dictates the spatial resolution. Thus, a sensitive element able to detect dielectric constant variations within small ranges is required. Note that a small encoder period is also convenient for identification purposes, in order to enhance the data density per unit length (DPL). In this work, the proposed sensing element is a microstrip line loaded with a transverse (linearly shaped) slot resonator and with a series capacitive gap. The slot resonator is very sensitive to variations in the dielectric constant of the material in contact with it, or surrounding it. Moreover, its elongated shape is very interesting in order to consider dielectric encoder inclusions of similar shape, thereby providing short dimensions in the direction of the chain axis, as required in near-field chipless-RFID systems with sequential bit reading. The topologies of the reader and encoder with all inclusions present at their predefined positions are depicted in Fig. 2.

Note that the type of encoders depicted in Fig. 2 cannot be easily read with a sensing element based on a microstrip line loaded with a CSR, as it was carried out in [18], or with a complementary split ring resonator (CSRR). The reason is the elongated shape of

the inclusions, unable to significantly modify the capacitance of the sensing resonant element (either CSR or CSRR), and consequently its resonance frequency. For this reason, the considered dielectric inclusions in [18] (apertures) exhibit a square shape and size comparable to the one of the CSR of the reader. By contrast, since the capacitance of the slot resonator is mainly determined by the dimensions of the narrow and long slot, and by the surrounding materials, it is expected that the presence of the inclusions depicted in Fig. 2 on top of the slot resonator significantly alters the capacitance and resonance of the sensing particle (the slot).

Additionally, the slot resonator exhibits higher sensitivity to resonance frequency variation, as compared to the one of the CSR, or CSRR. To demonstrate this, the lumped element equivalent circuit models of the slot- and CSR-loaded (or CSRR-loaded) microstrip line are considered (Fig. 3). In these models, L_c and C_c are the inductance and capacitance, respectively, of the bare resonators (i.e., without any material on top of it, or surrounding it), and C describes the coupling capacitance between the line and the CSR, or CSRR, in the corresponding circuit model. If we now consider that the resonant element is covered by a material under test (MUT), with dielectric constant ε_{MUT}, and that the thickness of such material is significantly larger than the transverse dimensions of the slots, the resonance frequency is given by [66]

$$f_o = \frac{1}{2\pi}\left\{L_c\left(C + C_c \frac{\varepsilon_r + \varepsilon_{MUT}}{\varepsilon_r + 1}\right)\right\}^{-1/2} \qquad (1)$$

where ε_r is the dielectric constant of the substrate (note that $C = 0$ pF for the slot-loaded line). The validity of (1) is also restricted to a substrate thickness much larger than transverse slot dimensions. These limitations relative to a minimum substrate and MUT thickness are necessary to guarantee that the electric field lines generated in the slots do not reach the opposite interface of the substrate or MUT,
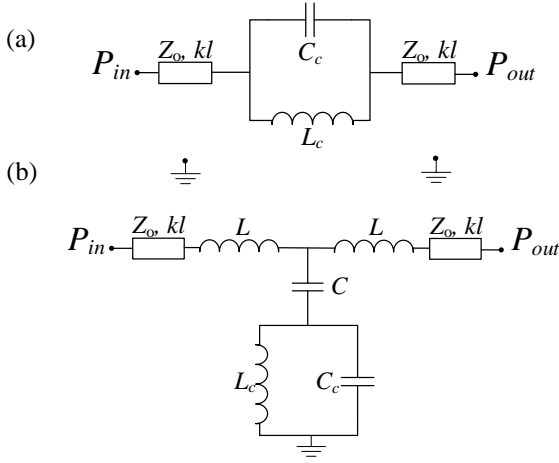
Fig. 3. Circuit model of the slot-loaded line (a) and CSR- or CSRR-loaded line (b). Z_0 and kl are the characteristic impedance and electrical length, respectively, of the access lines.

a necessary condition to express the slot capacitance of the resonator as shown in (1). In general, the presence of a thick enough MUT (or dielectric inclusion, the case of actual interest in this work) cannot be ensured. Nevertheless, this does not represent a loss of generality concerning the conclusions of the present analysis.

The relative sensitivity of resonance frequency with variations in the dielectric constant of the MUT is given by

$$S = \frac{1}{f_0}\frac{df_0}{d\varepsilon_{MUT}} \qquad (2)$$

and after some simple algebra, the following result is obtained:

$$S = -\frac{1}{2}\frac{C_c}{C_c(\varepsilon_r + \varepsilon_{MUT}) + C(\varepsilon_r + 1)} \qquad (3)$$

According to (3), the sensitivity increases by reducing C, and therefore it can be concluded that it is optimized in the slot-loaded line (where $C = 0$, as mentioned). Indeed, in this case, the relative sensitivity is found to be determined only by the dielectric constants of the substrate and MUT, according to

$$S = -\frac{1}{2(\varepsilon_r + \varepsilon_{MUT})} \qquad (4)$$

and it increases by decreasing the dielectric constant of the substrate (ε_{MUT} is not a design parameter).

For our purposes, we do not only need high frequency sensitivity, but also a high Q-factor. The reason is that the excursion of the transmission coefficient at the design (interrogation) frequency, which depends on both parameters, is expected to be enhanced by increasing S and Q. Note that a strong variation of the resonance frequency with ε_{MUT} (corresponding to high values of S) is not efficient in terms of transmission coefficient variation at a fixed frequency, if the bandwidth of the resonance is high (low Q-factor). Similarly, a high Q-factor (narrow notches) does not suffice to guarantee a minimum excursion of the transmission coefficient, if S is small. Thus, both S and Q need to be as large as possible. Decreasing ε_r enhances S, but it also reduces the Q-factor, as far as the resonator capacitance decreases.

The solution to this problem is to add an element to the slot-loaded line, i.e., a series gap, as illustrated in Fig. 2. The circuit model including the series gap is depicted in Fig. 4, where C_s is the capacitance of the gap and C_f accounts for the fringing capacitances. By including the series gap, a reflection zero (or transmission peak) located to the left of the resonance frequency of the slot is introduced. The reflection zero frequency is the one providing an image impedance, Z_I, identical to the reference impedance of the ports, Z_0. For a π-network with series impedance Z_s and shunt impedance Z_p, the image impedance is given by [67]

$$Z_I = Z_p\sqrt{\frac{Z_s}{Z_s + 2Z_p}} \qquad (5)$$

and the condition for total transmission ($Z_I = Z_0$) is

$$Z_s = 2\frac{Z_0^2 Z_p}{Z_p^2 - Z_0^2} \qquad (6)$$

In general, the fringing capacitance is small, providing a large value of Z_p. Thus, the reflection zero (or transmission peak) frequency can be approximated by the frequency satisfying $Z_s = 0$, that is

$$f_r = \frac{1}{2\pi}\left\{L_c\left(C_s + C_c\frac{\varepsilon_r + \varepsilon_{MUT}}{\varepsilon_r + 1}\right)\right\}^{-1/2} \qquad (7)$$

By choosing a small value of the capacitance C_s, the transmission peak can be situated very close to the transmission zero. According to (1) and (7), the presence of a MUT in contact to the slot resonator decreases both frequencies. Consequently, by setting the interrogation signal frequency to the peak frequency of the line loaded with the bare slot (i.e, $f_c = f_r|_{\varepsilon_{MUT}=1}$), it is expected to achieve a large excursion of the transmission coefficient when the slot resonator is loaded with a certain MUT (even in the case that the MUT is separated from the slot by an air gap, as required in a real scenario to avoid mechanical friction). By this means, the Q-factor of the slot resonator is not altered, but an abrupt transition in the response to the left of the transmission zero is achieved.

In the designed reader, the reflection and transmission zero frequencies with unloaded slot resonator are set to $f_r = 3.85$ GHz and $f_0 = 4.49$ GHz, respectively. This does not determine univocally the element values of the circuit model of the slot-loaded line with series gap, but this is an advantage, rather than a drawback, since extreme geometrical values can be avoided. For the design of the sensitive part of the reader, the following procedure has been followed: we have set the width of the slot to the minimum value (a convenient strategy to minimize the period of the dielectric inclusions, or encoder, chain). To enhance the Q-factor, the inductance of the slot should be minimized since the bandwidth of the slot resonator is proportional to L_c/C_c. For this reason, the considered topology of the sensitive resonator is a linear slot, rather than a dumbbell-shaped defect ground structure (DB-DGS). By tuning the slot length, we are able to vary its resonance frequency. Therefore, the length of the slot is dictated by the required resonance frequency, $f_0 = 4.49$ GHz, as indicated before. Then the gap distance is tuned until (i) the
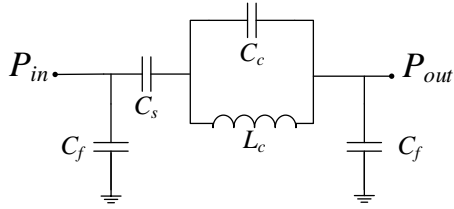
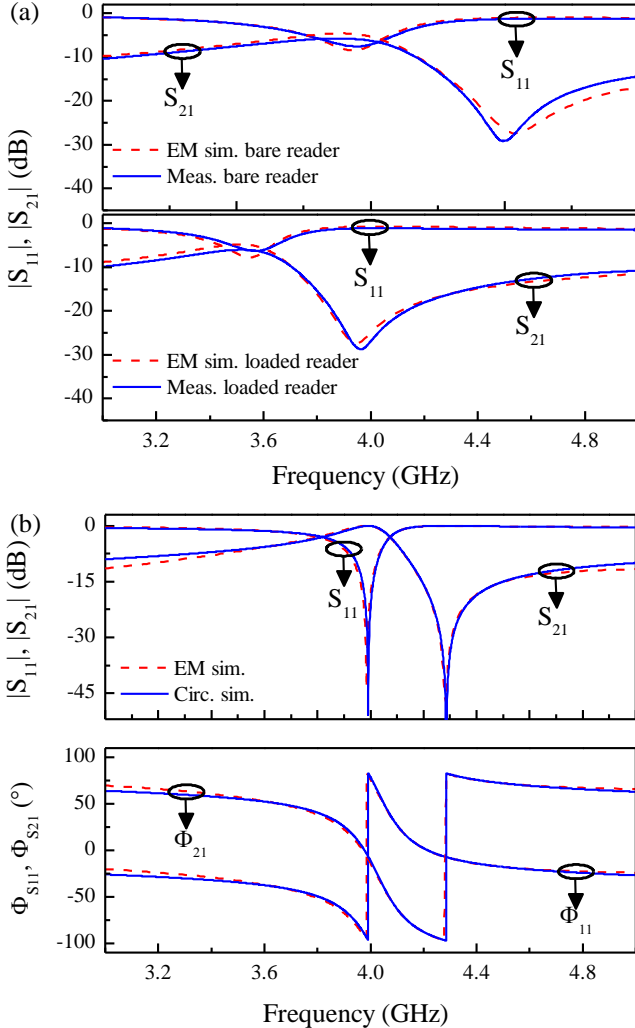Fig. 4. Circuit model of the slot-loaded line with series gap. Access lines are excluded in this model.

Fig. 5. Simulated (lossy) and measured responses of the bare reader and reader loaded with a dielectric slab with the dielectric constant and thickness indicated in the text (a), and frequency response of the bare reader inferred from lossless electromagnetic and circuit simulation of Fig 4 (b). Extracted element parameters are $C_s = 0.17$ pF, $L_c = 1.24$ nH, $C_c = 1.11$ pF, $C_f = 47.6$ fF. In (a), the excursion experienced by the insertion loss by loading the slot at the operating frequency $f_c = f_r|_{\varepsilon_{MUT}=1}$ is 14.3 dB.
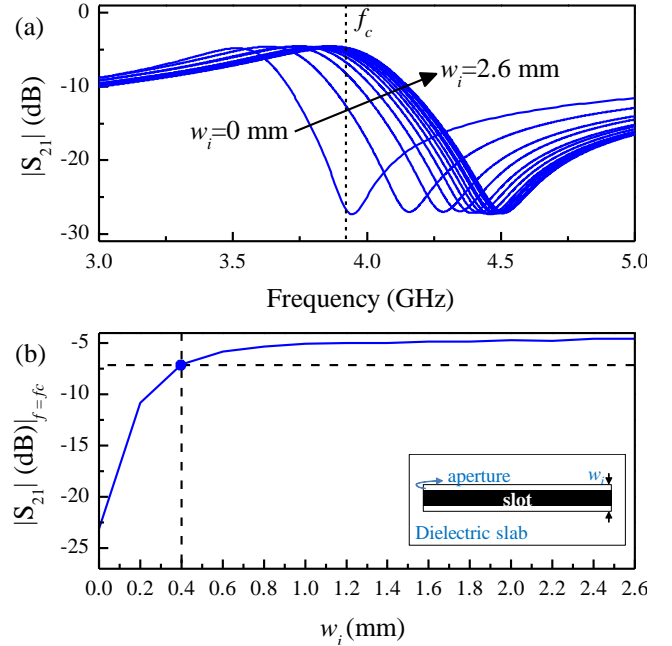

Fig. 6. Simulated frequency responses of the reader with a single aperture, obtained by varying the aperture width (a), and variation of the transmission coefficient at the operating frequency (b). The considered air gap is 0.2 mm.

reader substrate is the *Rogers RO4003* with thickness $h = 1.524$ mm, dielectric constant $\varepsilon_r = 3.55$ and loss tangent $\tan\delta = 0.0021$). Figure 5(b) depicts the response of the unloaded structure inferred from lossless full-wave electromagnetic simulation using *Keysight Momentum*. This response is compared with the response obtained by circuit simulation of the lumped model (also without losses), where the extracted parameters (indicated in the caption) have been considered. The agreement is very good, pointing out the validity of the model. Then we have simulated (including losses) the response by considering the slot loaded with a dielectric slab of thickness 0.635 mm, dielectric constant $\varepsilon_{MUT} = 10.2$ and loss tangent $\tan\delta = 0.0027$ (corresponding to the commercial *Rogers RO3010* substrate with such parameters), separated 0.2 mm (air gap) from the slot [Fig. 5(a)]. As expected, the overall response is shifted downwards, and a significant excursion of the transmission coefficient at the operating frequency, indicated in the caption of Fig. 5, is achieved.

IV. ENCODER DESIGN

In a first step towards the experimental validation of the proposed reader/encoder system (to be discussed in the next section), we have considered an all-dielectric encoder implemented by opening narrow apertures on the MUT of the previous section (*Rogers RO3010* substrate, with $h = 0.635$ mm and $\varepsilon_r = 10.2$). In order to determine the dimensions of the apertures and their separation, we have carried out a set of electromagnetic simulations including losses. In the first simulations, we have considered a single aperture of 24 mm length (identical to the length of the slot resonator), and we have simulated the frequency responses that result by varying the aperture width, with perfectly aligned aperture and slot. The results are depicted in Fig. 6(a), whereas Fig. 6(b) shows the variation of the

reflection zero with bare reader, $f_r|_{\varepsilon_{MUT}=1}$, is located as close as possible to the transmission zero, and (ii) the value of the transmission coefficient at $f_c = f_r|_{\varepsilon_{MUT}=1}$ is around -5 dB [Fig. 5(a)]. Such value is reasonable in order to obtain a large excursion of the transmission coefficient experienced by tag motion. It has been found that by setting $f_r|_{\varepsilon_{MUT}=1} = 3.85$ GHz, the value of -5 dB for the insertion loss is roughly obtained.

With the previous procedure, the dimensions indicated in the caption of Fig. 2 have been obtained (the considered
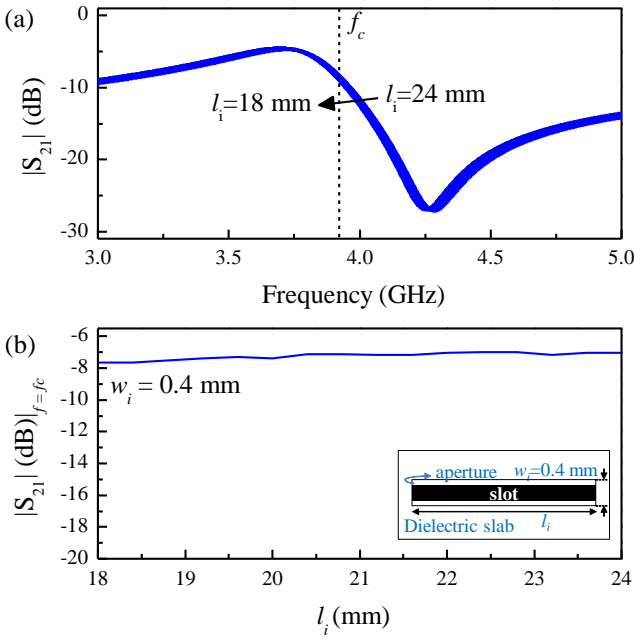
Fig. 7. Simulated frequency responses of the reader with a single aperture, obtained by varying the aperture length (a), and variation of the transmission coefficient at the operating frequency (b). The considered air gap is 0.2 mm.
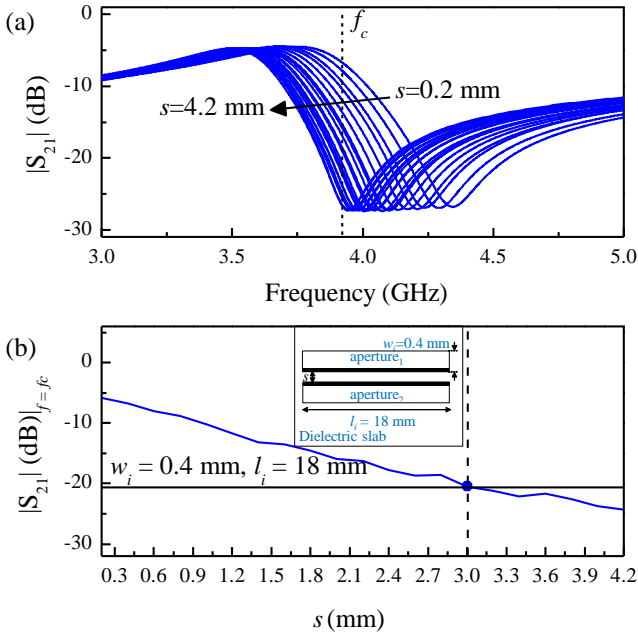

Fig. 8. Simulated frequency responses of the reader with a pair of apertures, obtained by varying the aperture separation (a), and variation of the transmission coefficient at the operating frequency (b). The considered air gap is 0.2 mm.
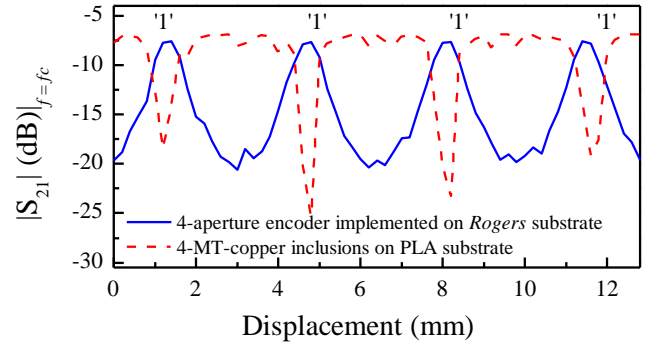

Fig. 9. Variation of the transmission coefficient at the operating frequency obtained by displacing a 4-aperture encoder implemented on commercial microwave substrate over the reader at 0.2 mm distance (air gap), and by displacing a 4-inclusion (of MT-copper) on PLA substrate over the reader at 0.075 mm distance.

transmission coefficient at the operating frequency, f_c. As the aperture widens, the response shifts up, towards the response corresponding to the bare reader. It is necessary to choose a value of the aperture width as small as possible, but providing a value of the transmission coefficient at f_c as close as possible to the value of the bare reader. Taking this tradeoff into account, and in view of Fig. 6(b), we have set the aperture width to 0.4 mm.

In order to determine the length of the apertures, we have carried out electromagnetic simulations by decreasing the length from the nominal value (in all the cases the width set to 0.4 mm). The results, depicted in Fig. 7, indicate that length reduction has negligible effect on the response, at least within the considered range. Therefore, the length of the apertures has been set to 18 mm, i.e., 6 mm shorter than the slot length.

Finally, in the third subset of electromagnetic simulations, we have analyzed the effects of aperture separation by considering a pair of apertures with the previously indicated dimensions, and variable distance. In this case, the two apertures are situated equidistantly from the slot resonator. The responses obtained from electromagnetic simulation by increasing the aperture separation are shown in Fig. 8(a), whereas Fig. 8(b) depicts the transmission coefficient at f_c. As expected, by increasing the aperture separation, the response tends to the one of the reader loaded with a uniform substrate. Reducing the apertures separation favors encoder resolution and data density, but at the expense of smaller dynamic range, (or excursion of the transmission coefficient at f_c). Thus, we have set the aperture separation to 3 mm. With this value, the period of the apertures chain is 3.4 mm, and the transmission coefficient at f_c is around −21 dB [see Fig. 8(b)]. This provides a variation in the transmission coefficient at the operating frequency (with and without aperture on top of the slot resonator) of roughly 14 dB, as corroborated in Fig. 9. This figure depicts the simulated transmission coefficient at f_c, obtained by displacing a 4-aperture encoder over the slot resonator. This excursion of the transmission coefficient is enough to provide a high modulation index, as required to read the encoder.

V. EXPERIMENTAL VALIDATION

A. Validation with Aperture Based Encoder Implemented on Commercial Microwave Substrate

The photograph of the fabricated reader and the one of a fabricated 50-aperture encoder (implemented on the *Rogers RO3010* substrate with thickness 0.635 mm, dielectric constant $\varepsilon_{MUT} = 10.2$ and loss tangent $\tan\delta = 0.0027$) are depicted in Fig. 10. In this first prototype encoder, all the apertures are present, since its potential application (taking into account the non-negligible cost of the considered encoder material) is the measurement of the relative
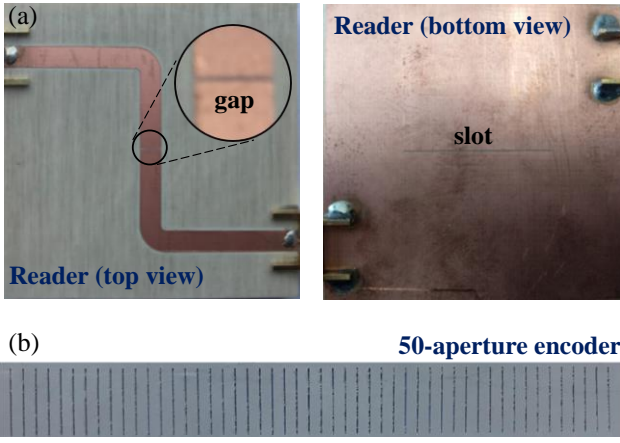
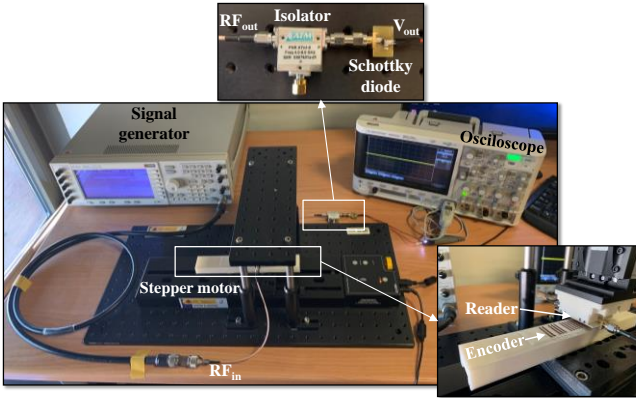Fig. 10. Photograph of the fabricated reader (a) and encoder (b).

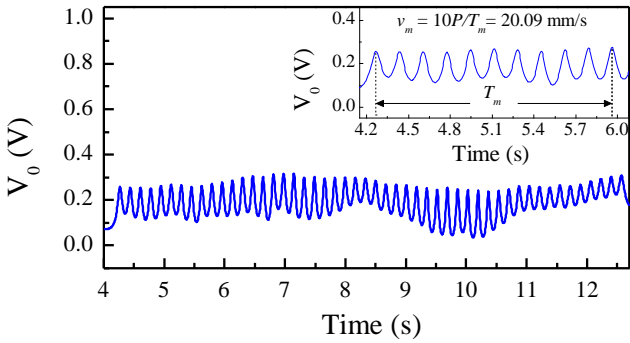Fig. 11. Experimental setup used for encoder reading.

Fig. 12. Measured envelope function for the fabricated 50-aperture encoder.

displacement and velocity between the reader and the encoder.

Before encoder reading, we have measured the response of the fabricated bare reader and the one with the considered substrate on top of the slot resonator (at 0.2 mm from it). Such responses, included in Fig. 5, show good agreement with the lossy electromagnetic simulations. Particularly, the simulated and measured reflection zero frequencies coincide to a good approximation.

For encoder reading, the frequency of the interrogation signal has been set to such (measured) reflection zero frequency, i.e., $f_c = 3.85$ GHz. As shown in Fig. 11, such interrogation signal is generated by means of a function generator (model *Agilent E4438C*) while an oscilloscope
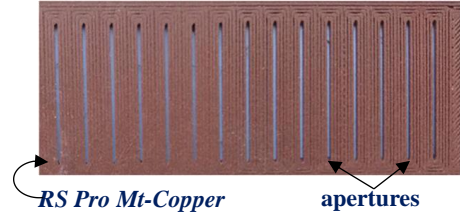

Fig. 13. Photograph of the 3D-printed encoder based on 15 apertures. The thickness of the printed slab is 0.65 mm.
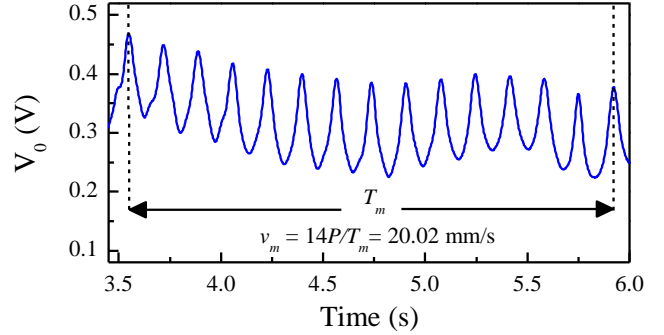

Fig. 14. Measured envelope function for the 15-aperture 3D-printed encoder.

(model *Agilent MSO-X 3104A*) is used to visualize the envelope function of the encoders. The relative motion between the reader and the encoder is achieved by means of a linear stepper motor (model *THORLABS LTS300/M*). Lastly, the envelope detector has been implemented by means of a Schottky diode (model *Avago HSMS-2860*), an active prove (model *Agilent N2795A*) with resistance and capacitance $R = 1$ MΩ and $C = 1$ pF, respectively, and an isolator (model *ATM PNR ATc4-8*) in order to prevent from unwanted reflections from de diode. The measured envelope function is depicted in Fig. 12. From the distance between adjacent peaks, or dips (both perfectly visible), the relative velocity between the encoder and the reader is inferred, provided the encoder period is well known. The displacement from a reference position is given by the cumulative number of periods in the envelope function, measured from that position. According to the results of Fig. 12, the averaged velocity over 10 periods has been found to be 20.09 mm/s, i.e., very similar to the nominal value (20 mm/s).

B. 3D-Printing Process and Materials

Let us now consider the implementation of 3D-printed encoders. For encoder fabrication, the *Ultimaker 3 Extended* 3D printer has been used. Fused filament fabrication (FFF) is the manufacturing technology used in such 3D printer. This is a 3D-printing process that uses a continuous filament of a thermoplastic material. According to specifications [68], this 3D-printer provides a lateral and vertical resolution of 12.5 μm and 2.5 μm, respectively. *PLA Polylactic acid* and *RS Pro MT-Copper* are the considered filaments used to fabricate the encoders. Before encoder fabrication, the electromagnetic properties of such filaments, i.e. the dielectric constant and the loss tangent, have been determined. To this end, the resonant cavity *Agilent 85072A* has been used. Square samples of 60 mm
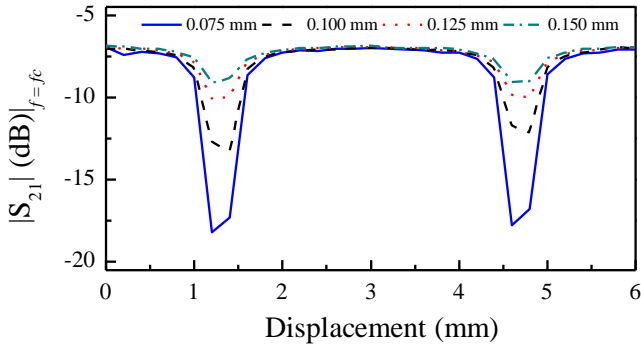
Fig. 15. Effects of the air gap variation on the transmission coefficient at f_c for the encoder based on MT-copper inclusions on PLA substrate. For time-consuming reasons, this tolerance analysis has been carried out through simulation by considering 2-MT copper inclusions on PLA substrate.

Code 110001110011111

RS Pro Mt-Copper **inclusions (ε_r = 7.6)**

PLA Polylactic acid (ε_r = 3)

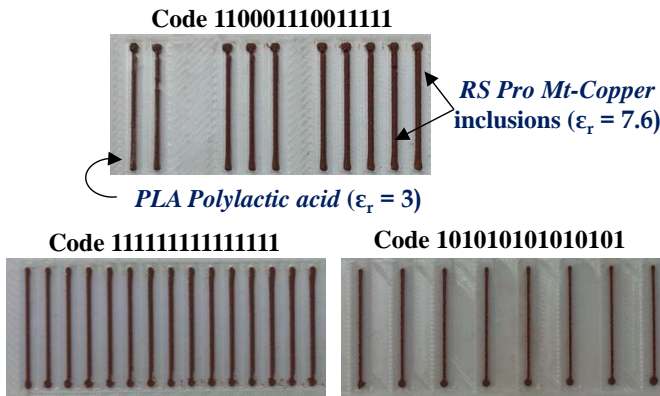**Code 111111111111111**   **Code 101010101010101**

Fig. 16. Photograph of 15-bit encoders with the indicated ID codes. The dimensions of the inclusions are length 18 mm and width 0.4 mm, whereas their separation is 3 mm (corresponding to an encoder period of 3.4 mm). The estimated thickness of the 3D-printed substrate is 0.2 mm, and the estimated thickness of the dielectric inclusions is 0.2 mm.

side length with a thickness of 1 mm have been 3D-printed with both types of filaments (these slab dimensions are those recommended by *Agilent*). The measured dielectric constant and loss tangent of *PLA Polylactic acid* are $\varepsilon_r = 3$ and $\tan\delta = 0.010$, respectively, whereas for *RS Pro MT-Copper* the values that have been obtained are $\varepsilon_r = 7.6$ and $\tan\delta = 0.015$. As will be shown next, such dielectric constant values are adequate to implement the two types of 3D-printed permittivity contrast encoders considered in this paper. We would like to mention that the resonant cavity *Agilent 85072A* is especially suited for the measurement of the permittivity and loss tangent of low-loss and thin film materials. Thus, for *RS Pro MT-Copper* (with copper content of 80% according to specifications), the loss tangent value inferred from the resonant cavity may be questionable. For this reason, we have compared the estimated loss tangent obtained by the resonant cavity with the one determined by means of a non-resonant transmission-line based method [69]. The measured loss tangent of *RS Pro MT-Copper* provided in [69] is roughly 0.016, which is in good agreement with the value obtained by means of the resonant cavity. Nevertheless, regardless of the loss factor and dielectric constant of *RS Pro MT-Copper*, the functionality of the fabricated encoders is demonstrated, as it will be shown in the next subsections.
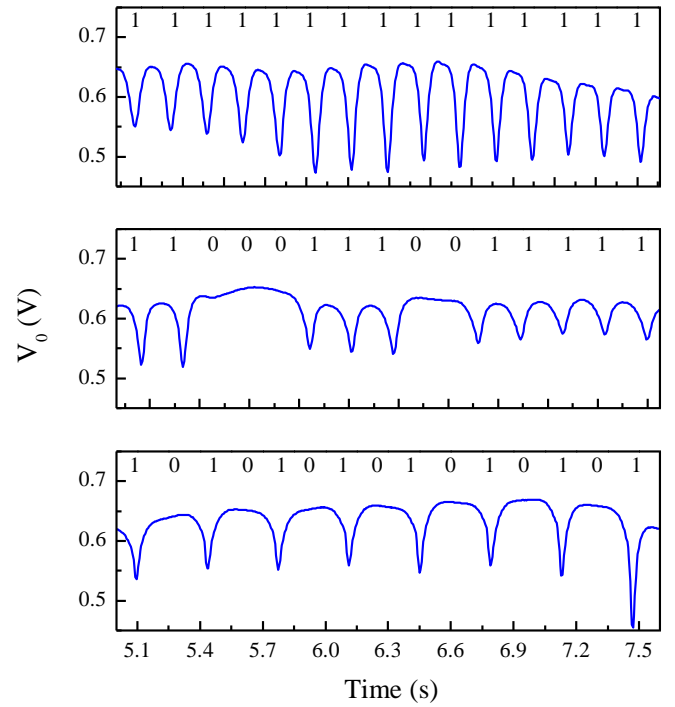

Fig. 17. Measured envelope functions for the 3D-printed encoders based on high dielectric constant inclusions (MT-copper).

C. Validation with Aperture Based 3D-Printed Encoders

Similar to the encoder shown in Fig. 10, in the first 3D-printed encoder implementation, the inclusions are also apertures, but made on a 3D-printed dielectric plate during fabrication. In this case, the considered filament is *RS Pro MT-Copper*. Since the value of the dielectric constant of this material is not very different from the one of the dielectric substrate of the encoder of Fig. 10, we expect that by fabricating 3D-printed encoders with identical aperture dimensions and separation (Fig. 13), the same reader can be useful for reading purposes. Figure 14 depicts the envelope function of the 3D-printed 15-aperture encoder that has been inferred by using the reader of Fig. 10, as well as the experimental setup used for reading the previous encoder. The presence of the apertures is clearly discerned as peaks in the envelope function. Therefore, the functionality of these 3D-printed encoders is demonstrated. It is important to highlight that despite the fact that the encoder materials are different than those of the encoder of Fig. 10, it has not been necessary to redesign the sensitive part of the reader. This is an important aspect related to system versatility, understood as the capability to use the reader in a variety of scenarios, including different types of encoders.

D. Validation with 3D-Printed Encoders Based on Dielectric Inclusions

In the second 3D-printed encoder realization, the inclusions are made of a high dielectric constant material 3D-printed on a dielectric substrate (also 3D-printed). Thus, the substrate has been printed by using *PLA Polylactic acid*, whereas the inclusions are strips of printed *RS Pro MT-Copper*. Before encoder implementation, we have simulated the transmission coefficient at f_c, achieved by displacing a 4-inclusions encoder over the slot resonator at 0.07 mm distance (air gap). The result, depicted in Fig. 9, indicates

that by reducing the airgap to 0.075 mm, it is possible to obtain a significant excursion of the transmission coefficient, necessary to properly read the encoder. In fact, the most important parameter influencing the performance of the proposed system is the air gap distance between the reader and the encoder. As the air gap increases, obviously, the reader is more insensitive to the presence of the encoder, and the dynamic range decreases. The effects of the air gap variation on the excursion of the transmission coefficient are depicted in Fig. 15. According to these results, the guiding system for encoder motion should ensure a maximum air gap of the order of 0.1 mm while the encoder is being displaced over the sensitive part of the reader (this seems to be feasible in a real scenario).

The photograph of a set of 3D-printed 15-bit encoders with different ID codes is depicted in Fig. 16, where dimensions are indicated (see caption). We have read these encoders by means of the designed reader and experimental setup available in our laboratory (indicated before). The results, depicted in Fig. 17, reveal that the different encoders are correctly read. Note, however, that in these encoders the permittivity contrast is complementary to the one of the previous encoders; that is, the inclusions are made of a high dielectric constant material, whereas the dielectric constant of the substrate is comparatively small. By contrast, in the previous encoders, the inclusions are apertures (with $\varepsilon_r = 1$) made on a high dielectric constant material (substrate). For this reason, the presence of inclusions on top of the slot resonator of the reader provides a dip, rather than a peak, in the envelope functions (see Fig. 17), contrary to the encoders based on apertures (see Figs. 12 and 14). For this same reason, the response in Fig. 9 corresponding to the encoder based on MT-copper inclusions is complementary to the one of the encoder based on apertures.

VI. Discussion

As compared to the all-dielectric encoders reported in [18], the proposed encoders exhibit a smaller period. This has direct impact on spatial resolution, in the application of the reader/encoder system as linear displacement sensor. Concerning the data density per unit surface (DPS) and per unit length (DPL), the achieved values are DPS = 1.66 bit/cm^2 and DPL = 2.99 bit/cm (50% higher as compared to the design proposed in [18]), respectively. As discussed in previous papers [15],[16], the DPL (rather than the DPS) is the key data density parameter in encoders based on chains of inclusions, and intended to be used as near-field chipless-RFID tags. The reason is that the shape factor is extremely elongated if the number of bits is high and the DPL is moderate or small. Therefore, the reduction of the period of all-dielectric encoders is essential for both applications. For that purpose, the strategy has been to consider a reader able to detect the presence or absence of very small inclusions in the direction of the chain axis (i.e., transversally oriented linear apertures or dielectric strips). Note that the width of the inclusions in the encoders reported in this paper is as small as 0.4 mm. Nevertheless, the required separation between the inclusions, for proper discernment of their presence or absence, is 3 mm (as it has been justified in the previous section), providing an encoder period of 3.4 mm.

This period is not as small as the one achieved in encoders based on chains of transversally oriented metallic strips [15],[16], where a period as small as 0.6 mm was achieved. The reason is that metals are more efficient than dielectrics in modifying the capacitance of a resonant element through non-contact. Namely, since dielectrics do not "absorb" the electric field lines, as metals do, they need more spatial extension than metals in order to produce the same capacitance (and hence resonance frequency) variation.

According to the previous words, the reported all-dielectric permittivity contrast encoders cannot compete against encoders based on metallic inclusions (etched or printed) in terms of resolution and data density. However, metallic elements are sensitive to wearing and aging effects, potentially caused by chafing, rubbing, etc. Thus, the reported encoders are a good option in applications where a long-life use is required, at the expense of more limited performance as compared to metallic-based encoders.

Concerning encoder cost, the estimated material cost of the 3D-printed encoder based on apertures is 0.05 € (using MT-copper), whereas the material cost of the one fabricated on the *Rogers* substrate is 4.78 €. On the other hand, with regard to the encoders based on dielectric inclusions, the cost of the materials (*PLA Polylactic acid and RS Pro MT-Copper*) is roughly two orders of magnitude cheaper than the cost of conductive inks (in this case the comparison should be made with tags based on printed metallic inclusions), since the cost of 1 kg of ceramic based filaments used and the Dupont^{TM} PE410 conductive ink (which was used in [13] by the authors) are around 80 € and 14000 €, respectively. However, inkjet-printed metallic tags on ordinary paper substrates (as demonstrated in [13]) are very cheap, owing to the cost of ordinary paper, and to the fact that an extremely small amount of ink, i.e., a single layer, suffices for tag functionality. Nevertheless, the estimated material cost of the 3D-printed 15-bit encoder based on dielectric inclusions is 0.04 €, while the estimated material cost of 15-bit inkjet-printed encoder on ordinary paper is 0.12 €. This aspect demonstrates that all-dielectric encoders are cheaper than encoders based on metallic inclusions. Specifically, the cost of all-dielectric encoders corresponds to a reduction of roughly 67% of the cost of metallic-inclusion based encoders.

The implementation of 3D-printed all-dielectric encoders on paper substrate is left for future works. Nevertheless, it should be taken into account that 3D-printing encoding can be directly carried out during manufacturing of 3D-printed products, e.g., by generating an ID code based on apertures or on dielectric inclusions. This does not represent an extra production cost, and, at the same time, the use of a dedicated tag is avoided. Obviously, the use of optical barcodes is a very low cost alternative (extremely extended nowadays). However, such barcodes may be subjected to wearing, can be manipulated, and their data capacity is limited. By contrast, in the proposed encoders, the number of bits is only limited by encoder size and encoder implementation in the considered item or product offers very high robustness against mechanical wearing and exposure to harsh environments (e.g., contacting the products with water or liquids does not deteriorate the encoder). Thus, the reported 3D-printing approach for

encoder fabrication may be of interest in various scenarios. To the best of our knowledge, it is the first time that 3D-printed all-dielectric electromagnetic encoders based on permittivity contrast are reported.

VII. CONCLUSIONS

In conclusion, full 3D-printed all-dielectric electromagnetic encoders based on permittivity contrast have been reported in this paper. The encoders consist of a chain of dielectric inclusions on a host dielectric material with significantly different dielectric constant. We have considered two types of encoders: (i) those where the inclusions are simple apertures, and (ii) those where the inclusions are high dielectric constant materials. For encoder reading, a specifically designed reader based on a microstrip line loaded with a slot resonator (the sensitive part) and a series gap has been used, and the functionality of the system for 3D-printed encoders with 3.4 mm resolution has been demonstrated. These encoders can be used as sensing elements for motion control applications (to measure the relative displacement and velocity between the encoder and the reader), or as tags in near-field chipless-RFID applications, where the presence or absence of inclusions at predefined positions is used for coding purposes. Major robustness against mechanical wearing and aging, as compared to electromagnetic encoders based on printed metallic inclusions, is an advantage of the reported encoders. The cost of the considered 3D-printing materials is by far smaller than the one of commercial conductive inks. Thus, low price encoders can be implemented through the reported approach, at least as compared to rigid encoders based on commercial microwave substrates. For certain 3D-printed products (e.g., those based on dielectric materials), the reported encoders can be directly implemented during manufacturing of the item to be tagged. This is an additional, and important, advantage, as far as dedicated tags are avoided, object coding does not represent extra production costs, and item exposure to aggressive or hostile environments does not jeopardize the functionality of the encoders. For instance, direct encoding of 3D-printed objects during manufacturing provides an intrinsically water-resistant encoding system.

REFERENCES

[1] E. Eitel, "Basics of rotary encoders: overview and new technologies", *Machine Design Magazine*, 7 May 2014.

[2] G. K. McMillan, D.M. Considine, Eds., *Process Instruments and Controls Handbook*, Fifth Edition, McGraw Hill 1999, ISBN 978-0-07-012582-7, page 5.26.

[3] X. Li, J. Qi, Q. Zhang, and Y. Zhang, "Bias-tunable dual-mode ultraviolet photodetectors for photoelectric tachometer," *Appl. Phys. Lett.*, vol. 104, no. 4, pp. 041108-1–041108-4, Jan. 2014.

[4] J. Naqui, F. Martín, "Application of broadside-coupled split ring resonator (BC-SRR) loaded transmission lines to the design of rotary encoders for space applications", *IEEE MTT-S Int. Microw. Symp.* (IMS'16), San Francisco, May 2016.

[5] J. Mata-Contreras, C. Herrojo, and F. Martín, "Application of split ring resonator (SRR) loaded transmission lines to the design of angular displacement and velocity sensors for space applications", *IEEE Trans. Microw. Theory Techn.*, vol. 65, no. 11, pp. 4450-4460, Nov. 2017.

[6] C. Herrojo, J. Mata-Contreras, F. Paredes, F. Martín, "Microwave encoders for chipless RFID and angular velocity sensors based on S-shaped split ring resonators (S-SRRs)", *IEEE Sensors J.*, vol. 17, pp. 4805-4813, Aug. 2017.

[7] J. Mata-Contreras, C. Herrojo, and F. Martín, "Detecting the rotation direction in contactless angular velocity sensors implemented with rotors loaded with multiple chains of split ring resonators (SRRs)", *IEEE Sensors J.*, vol.18, no. 17, pp. 7055-7065, Sep. 2018.

[8] C. Herrojo, J. Mata-Contreras, F. Paredes, Ferran Martín, "Near-Field Chipless RFID Encoders with Sequential Bit Reading and High Data Capacity", *IEEE MTT-S Int. Microw. Symp.* (IMS'17), Honolulu, Hawaii, Jun. 2017.

[9] C. Herrojo, J. Mata-Contreras, F. Paredes, F. Martín, "High data density and capacity in chipless radiofrequency identification (chipless-RFID) tags based on double-chains of S-shaped split ring resonators (S-SRRs)", *EPJ Appl. Metamat.*, vol. 4, article 8, 6 pages, Oct. 2017.

[10] C. Herrojo, J. Mata-Contreras, F. Paredes, Ferran Martín, "Near-field chipless RFID system with high data capacity for security and authentication applications", *IEEE Trans. Microw. Theory Techn.*, vol. 65 (12), pp. 5298-5308, Dec. 2017.

[11] C. Herrojo, J. Mata-Contreras, F. Paredes, A. Núñez, E. Ramon, and F. Martín, "Near-field chipless-RFID system with erasable/programable 40-bit tags inkjet printed on paper substrates", *IEEE Microw. Wireless Compon. Lett.*, vol. 28, pp. 272-274, Mar. 2018.

[12] C. Herrojo, J. Mata-Contreras, F. Paredes, A. Núñez, E. Ramón, F. Martín, "Near-field chipless-RFID tags with sequential bit reading implemented in plastic substrates", *Int. J. Magnetism Magnet. Mat.*, vol. 459 pp. 322–327, 2018.

[13] C. Herrojo, M. Moras, F. Paredes, A. Núñez, E. Ramón, J. Mata-Contreras, F. Martín, "Very low-cost 80-bit chipless-RFID tags inkjet printed on ordinary paper", *Technologies*, vol. 6, p. 52, 2018.

[14] J. Havlicek, C. Herrojo, J. Mata-Contreras, F. Paredes, F. Martín, "Enhancing the data density in near-field chipless-RFID systems", *2018 IEEE MTT-S Latin America Microw. Conf.* (LAMC 2018), Arequipa, Perú, Dec. 12-14, 2018.

[15] J. Havlíček, C. Herrojo, F. Paredes, J. Mata-Contreras, F. Martín, "Enhancing the per-unit-length data density in near-field chipless-RFID systems with sequential bit reading", *IEEE Ant. Wireless Propag. Lett.*, vol. 18, pp. 89-92, Jan. 2019.

[16] C. Herrojo, F. Muela, J. Mata-Contreras, F. Paredes, F. Martín, "High-density microwave encoders for motion control and near-field chipless-RFID", *IEEE Sensors J.*, vol. 19, pp. 3673-3682, May 2019.

[17] C. Herrojo, F. Paredes, J. Mata-Contreras, E. Ramon, A. Núñez, F. Martín, "Time-domain signature barcodes: near-field chipless-RFID systems with high data capacity" *IEEE Microw. Mag.*, to be published.

[18] C. Herrojo, F. Paredes, J. Mata-Contreras, F. Martín, "All-dielectric electromagnetic encoders based on permittivity contrast for displacement/velocity sensors and chipless-RFID tags", *IEEE-MTT-S Int. Microw. Symp.* (IMS'19), Boston (MA), USA, June 2019.

[19] S. Preradovic and N. C. Karmakar, "Chipless RFID: bar code of the future," *IEEE Microw. Mag.*, vol. 11, pp. 87-97, 2010.

[20] S. Preradovic and N. C. Karmakar, *Multiresonator-Based Chipless RFID: Barcode of the Future*, Springer, 2011.

[21] I. Jalaly and I. D. Robertson, "RF barcodes using multiple frequency bands," *IEEE MTT-S Int. Microw. Symp.*, Long Beach, USA, Jun. 2005, pp. 139–142.

[22] S. Preradovic, I. Balbin, N. C. Karmakar, and G. Swiegers, "A novel chipless RFID system based on planar multiresonators for barcode replacement," 2008 *IEEE Int. Conf. RFID*, Apr. 2008, pp. 289–296.

[23] S. Preradovic, I. Balbin, N. C. Karmakar, and G. F. Swiegers, "Multiresonator-based chipless RFID system for low-cost item tracking," *IEEE Trans. Microw. Theory Techn.*, vol. 57, pp. 1411-1419, 2009.

[24] S. Preradovic and N. C. Karmakar, "Design of chipless RFID tag for operation on flexible laminates," *IEEE Anten. Wireless Propag. Lett.*, vol. 9, pp. 207-210, 2010.

[25] J. McVay, A. Hoorfar, and N. Engheta, "Space-filling curve RFID tags," *2006 IEEE Radio Wireless Symp.*, pp. 199–202.

[26] I. Jalaly and D. Robertson, "Capacitively-tuned split microstrip resonators for RFID barcodes," *2005 European Microwave Conference*, Oct. 2005, vol. 2, pp. 4–7.

[27] H.-S. Jang, W.-G. Lim, K.-S. Oh, S.-M. Moon, and J.-W. Yu, "Design of low-cost chipless system using printable chipless tag with electromagnetic code", *IEEE Microw. Wireless Compon. Lett.*, vol. 20, pp. 640-642, 2010.

[28] A. Vena, E. Perret, and S. Tedjini, "A fully printable chipless RFID tag with detuning correction technique", *IEEE Microw. Wireless Compon. Lett.*, vol. 22(4), pp. 209-211, 2012.

[29] A. Vena, E. Perret, and S. Tedjini, "Design of compact and auto-compensated single-layer chipless RFID tag", *IEEE Trans. Microw. Theory Techn.*, vol. 60(9), pp. 2913-2924, Sep. 2012.

[30] A. Vena, E. Perret, and S. Tedjini, "High-capacity chipless RFID tag insensitive to the polarization", *IEEE Trans. Ant. Propag.*, vol. 60(10), pp. 4509-4515, Oct. 2012.

[31] D. Girbau, J. Lorenzo, A. Lazaro, C. Ferrater, and R. Villarino, "Frequency-coded chipless RFID tag based on dual-band resonators," *IEEE Ant. Wireless Propag. Lett.*, vol. 11, pp. 126–128, 2012.

[32] M. M. Khan, F. A. Tahir, M. F. Farooqui, A. Shamim, H. M. Cheema, "3.56-bits/cm^2 compact inkjet printed and application specific chipless RFID tag," *IEEE Ant. Wireless Propag. Lett.*, vol. 15, pp. 1109-1112, 2016.

[33] R. Rezaiesarlak and M. Manteghi, "Complex-natural-resonance-based design of chipless RFID tag for high-density data," *IEEE Trans. Ant. Propag.*, vol. 62, pp. 898-904, Feb. 2014.

[34] M. S. Bhuiyan and N. Karmakar, "A spectrally efficient chipless RFID tag based on split-wheel resonator," in *Int. Antenna Technol. Workshop on Small Antennas, Novel EM Struct., Mater., Appl.*, 2014, pp. 1–4.

[35] C. M. Nijas *et al.*, "Low-cost multiple-bit encoded chipless RFID tag using stepped impedance resonator," *IEEE Trans. Ant. Propag.*, vol. 62, no. 9, pp. 4762–4770, Sep. 2014.

[36] J. Machac and M. Polivka, "Influence of mutual coupling on performance of small scatterers for chipless RFID tags," *24th Int. Radioelektron. Conf.*, 2014, pp. 1–4.

[37] M. Khaliel, A. El-Awamry, A. Fawky, M. El-Hadidy, and T. Kaiser, "A novel co/cross-polarizing chipless RFID tags for high coding capacity and robust detection," *2015 IEEE Int. Symp. Ant. Propag. & USNC/URSI National Radio Sci. Meeting*, Jul. 2015, pp. 159–160.

[38] M. Svanda, J. Machac, M. Polivka, J. Havlicek., "A comparison of two ways to reducing the mutual coupling of chipless RFID tag scatterers," in Proc. of *21st International Conference on Microwave, Radar and Wireless Communications (MIKON)*, May 2016, pp. 1-4.

[39] C. Herrojo, J. Naqui, F. Paredes and F. Martín, "Spectral signature barcodes based on S-shaped Split ring resonators (S-SRR)", *EPJ Applied Metamaterials*, vol. 3, pp. 1-6, Jun. 2016.

[40] A. Vena, E. Perret, S. Tedjini, "Chipless RFID tag using hybrid coding technique," *IEEE Trans. Microw. Theory Techn.*, vol. 59, pp. 3356-3364, Dec. 2011.

[41] A. Vena, E. Perret, S. Tedjini, "A compact chipless RFID tag using polarization diversity for encoding and sensing", *2012 IEEE Int. Conf. RFID*, pp. 191-197, 2012.

[42] M. A. Islam and N. C. Karmakar, "A novel compact printable dual-polarized chipless RFID system," *IEEE Trans. Microw. Theory Techn.*, vol. 60, pp. 2142-2151, Jul. 2012.

[43] I. Balbin, N.C. Karmakar, "Phase-encoded chipless RFID transponder for large scale low cost applications", *IEEE Microw. Wireless. Compon. Lett.*, vol. 19, pp. 509-511, 2009.

[44] S. Genovesi, F. Costa, A. Monorchio, G. Manara, "Chipless RFID tag exploiting multifrequency delta-phase quantization encoding", *IEEE Ant. Wireless Propag. Lett.*, vol. 15, pp. 738-741, 2015.

[45] O. Rance, R. Siragusa, P. Lemaitre-Auger, and E. Perret, "RCS magnitude coding for chipless RFID based on depolarizing tag," in *IEEE MTT-S Int. Microw. Symp. Dig.*, 2015, pp. 1–4.

[46] O. Rance, R. Siragusa, P. Lemaître-Auger, E. Perret, "Toward RCS magnitude level coding for chipless RFID," *IEEE Trans. Microw. Theory Techn.*, vol. 64, pp. 2315-2325, Jul. 2016.

[47] C. Herrojo, J. Naqui, F. Paredes, F. Martín, "Spectral signature barcodes implemented by multi-state multi-resonator circuits for chipless RFID tags", *IEEE MTT-S International Microwave Symposium* (IMS'16), San Francisco, May 2016.

[48] C. Herrojo, F. Paredes, J. Mata-Contreras, S. Zuffanelli and F. Martín, "Multi-state multi-resonator spectral signature barcodes implemented by means of S-shaped split ring resonators (S-SRR)", *IEEE Trans. Microw. Theory Techn.*, vol. 65, no. 7, pp. 2341-2352, Jul. 2017.

[49] C. Feng, W. Zhang, L. Li, L. Han, X. Chen, and R. Ma, "Angle-based chipless RFID tag with high capacity and insensitivity to polarization," *IEEE Trans. Ant. Propag.*, vol. 63, no. 4, pp. 1789–1797, Apr. 2015.

[50] A. El-Awamry, M. Khaliel, A. Fawky, M. El-Hadidy, and T. Kaiser, "Novel notch modulation algorithm for enhancing the chipless RFID tags coding capacity," in *IEEE Int. RFID Conf.*, 2015, pp. 25–31.

[51] A. Vena, A. A. Babar, L. Sydanheimo, M. M. Tentzeris, and L. Ukkonen, "A novel near-transparent ASK-reconfigurable inkjet-printed chipless RFID tag," *IEEE Ant. Wireless Propag. Lett.*, vol. 12, pp. 753–756, 2013.

[52] A. Chamarti and K. Varahramyan, "Transmission delay line based ID generation circuit for RFID applications," *IEEE Microw. Wireless Compon. Lett.*, vol. 16, pp. 588-590, 2006.

[53] J. Vemagiri, A. Chamarti, M. Agarwal, and K. Varahramyan, "Transmission line delay-based radio frequency identification (RFID) tag," *Microw. Opt. Technol. Lett.*, vol. 49, no. 8, pp. 1900–1904, Aug. 2007.

[54] M. Schüßler, C. Damm, and R. Jakoby, "Periodically LC loaded lines for RFID backscatter applications," *Proc. Metamaterials 2007*, Rome, Italy, October 2007, pp. 103-106.

[55] M. Schüßler, C. Damm, M. Maasch, and R. Jakoby, "Performance evaluation of left-handed delay lines for RFID backscatter applications," *IEEE MTT-S Int. Microw. Symp. 2008*, pp. 177-180.

[56] F.J. Herraiz-Martínez, F. Paredes, G. Zamora, F. Martín, and J. Bonache, "Printed magnetoinductive-wave (MIW) delay lines for chipless RFID applications", *IEEE Trans. Ant. Propag.*, vol. 60, pp. 5075-5082, Nov. 2012.

[57] L. Zhang, S. Rodriguez, H. Tenhunen, and L.-R. Zheng, "An innovative fully printable RFID technology based on high speed time-domain reflections," *Conference on High Density Microsystem Design and Packaging and Component Failure Analysis, 2006. HDP '06.*, Shanghai, China, Jun. 2006, pp. 166–170.

[58] L. Zhang, S. Rodriguez, L. Zhang, B. Shao, and L.-R. Zheng, "Design and implementation of a fully reconfigurable chipless RFID tag using Inkjet printing technology," *2008 IEEE Int. Symp. Circuits Syst.*, Seattle, USA, May 2008, pp. 1524–1527.

[59] C. Mandel, M. Schussler, M. Maasch, and R. Jakoby, "A novel passive phase modulator based on LH delay lines for chipless microwave RFID applications," *2009 IEEE MTT-S Int. Microw. Work. Wireless Sensing, Local Positioning, RFID*, Cavtat, Croatia, Sep. 2009, pp. 1–4.

[60] R. Nair, E. Perret, and S. Tedjini, "Temporal multi-frequency encoding technique for chipless RFID applications," *IEEE MTT-S Int. Microw. Symp.*, Montreal, Canada, Jun. 2012, pp. 1–3.

[61] S. Gupta, B. Nikfal, and C. Caloz, "RFID system based on pulse-position modulation using group delay engineered microwave C-sections," *2010 Asia-Pacific Microw. Conf.*, Dec. 2010, pp. 203–206.

[62] E. G. Cristal, "Analysis and exact synthesis of cascaded commensurate transmission-line C-Section all-pass networks," *IEEE Trans. Microw. Theory Tech.*, vol. 14, no. 6, pp. 285–291, Jun. 1966.

[63] S. Gupta, B. Nikfal, and C. Caloz, "Chipless RFID system based on group delay engineered dispersive delay structures," *IEEE Ant. Wirel. Propag. Lett.*, vol. 10, no. 2, pp. 1366–1368, Dec. 2011.

[64] R. S. Nair, E. Perret, and S. Tedjini, "Group delay modulation for pulse position coding based on periodically coupled C-sections," *Annals of Telecommunications*, vol. 68, no. 7–8, pp. 447–457, Aug. 2013.

[65] R. Nair, E. Perret, and S. Tedjini, "Chipless RFID based on group delay encoding," *2011 IEEE International Conference on RFID-Technologies and Applications*, vol. 1, pp. 214–218, Sep. 2011.

[66] L. Su, J. Mata-Contreras, P. Vélez, A. Fernández-Prieto, and F. Martín, "Analytical method to estimate the complex permittivity of oil samples", *Sensors*, vol. 18, p. 984, 2018.

[67] F. Martín, *Artificial Transmission Lines for RF and Microwave Applications*, John Wiley, Hoboken, NJ, 2015.

[68] Ultimaker, "Ultimaker 3 specifications", datasheet.

[69] J. Muñoz-Enano, P. Vélez, M. Gil and F. Martín, "An Analytical Method to Implement High Sensitivity Transmission Line Differential Sensors for Dielectric Constant Measurements," *IEEE Sensors J.*, to be published, doi: 10.1109/JSEN.2019.2941050.

Cristian Herrojo was born in Barcelona, Spain, in 1983. He received the Telecommunications Technical Engineering degree in electronic systems and Telecommunications Engineering degree from the Universitat Autònoma de Barcelona in 2010 and 2012, respectively and the PhD degree in Electronics Engineering from the same university in 2018. His research interests include RF/microwave devices, Chipless-RFID and RFID technology, and Metamaterials.

Ferran Paredes was born in Badalona (Barcelona), Spain in 1983. He received the Telecommunications Engineering Diploma (specializing in Electronics) and the Telecommunications Engineering degree from the Universitat Autònoma de Barcelona in 2004 and 2006, respectively and the PhD degree in Electronics Engineering from the same university in 2012. He was Assistant Professor from 2006 to 2008 at the Universitat Autònoma de Barcelona, where he is currently working as a Research Assistant. His research interests include metamaterial concepts, passive microwaves devices, antennas and RFID.

Jordi Bonache was born in Cardona (Barcelona), Spain, in 1976. He received the Physics and Electronics Engineering degrees and the Ph.D. in electronics engineering from the Universitat Autònoma de Barcelona, in 1999, 2001 and 2007, respectively. In 2000, he joined the High Energy Physics Institute of Barcelona, where he was involved in the design and implementation of the control and monitoring system of the MAGIC telescope. In 2001, he joined the Department of Electronics Engineering, Universitat Autònoma de Barcelona, where he is currently Professor of Electronics. From 2006 to 2009, he was an Executive Manager with CIMITEC, Bellaterra, Spain, where he is currently a Project Manager and leads the research on RFID and antennas. His current research interests include active and passive microwave devices, metamaterials, antennas and RFID.

Ferran Martín (M'04-SM'08-F'12) was born in Barakaldo, Spain, in 1965. He received the B.S. degree in physics and Ph.D. degree from the Universitat Autònoma de Barcelona (UAB), Barcelona, Spain, in 1988 and 1992, respectively. From 1994 to 2006 he was Associate Professor in Electronics at the Departament d'Enginyeria Electrònica (Universitat Autònoma de Barcelona), and since 2007 he is Full Professor of Electronics. His research activity has been very broad, including the modelling and simulation of electron devices for high frequency applications, millimeter wave and THz generation systems, the application of electromagnetic bandgaps to microwave and millimeter wave circuits, and the application of metamaterial concepts to the miniaturization and optimization of microwave circuits and antennas. He is now very active in the development of microwave sensors for dielectric characterization and motion control, and also in the topic of chipless-RFID. He is the head of the Microwave Engineering, Metamaterials and Antennas Group (GEMMA Group) at UAB, and director of CIMITEC, a research Center on Metamaterials supported by TECNIO (Generalitat de Catalunya). He has organized several international events related to metamaterials, including Workshops at the IEEE International Microwave Symposium (years 2005 and 2007) and European Microwave Conference (years 2009, 2015, 2017, and 2018), and the Fifth International Congress on Advanced Electromagnetic Materials in Microwaves and Optics (Metamaterials 2011), where he has acted as chair of the Local Organizing Committee. He has acted as Guest Editor in several Special Issues, mainly related to Metamaterials, in various International Journals. He has authored and co-authored over 580 technical conference, letter, journal papers and book chapters, he is co-author of the book on Metamaterials entitled *Metamaterials with Negative Parameters: Theory, Design and Microwave Applications* (John Wiley & Sons Inc. 2008), author of the book *Artificial Transmission Lines for RF and Microwave Applications* (John Wiley & Sons Inc. 2015), co-editor of the book *Balanced Microwave filters* (John Wiley & Sons Inc. and IEEE-Press, 2018), and co-author of the book *Time-Domain Signature Barcodes for Chipless-RFID and Sensing Applications* (Springer, to be published in 2020). Ferran Martín has generated 19 PhDs, he has filed several patents on metamaterials, and he has headed dozens of Development Contracts.

Prof. Martín is a member of the IEEE Microwave Theory and Techniques Society (IEEE MTT-S). He is reviewer of the *IEEE Transactions on Microwave Theory and Techniques* and *IEEE Microwave and Wireless Components Letters*, among many other journals, and he serves as member of the Editorial Board of *IET Microwaves, Antennas and Propagation*, *International Journal of RF and Microwave Computer-Aided Engineering* and *Sensors*. He is also a member of the Technical Committees of the European Microwave Conference (EuMC) and International Congress on Advanced Electromagnetic Materials in Microwaves and Optics (Metamaterials). Among his distinctions, Ferran Martín has received the 2006 Duran Farell Prize for Technological Research, he holds the *Parc de Recerca UAB – Santander* Technology Transfer Chair, and he has been the recipient of three ICREA ACADEMIA Awards (calls 2008, 2013 and 2018). He is Fellow of the IEEE since 2012 and Fellow of the IET since 2016.